REPORT DOCUMENTATION PAGE

Form Approved
OMB No. 0704-0188

1. REPORT DATE *(DD-MM-YYYY)*	**2. REPORT TYPE**	**3. DATES COVERED** *(From - To)*
2007	Conference Paper POSTPRINT	2006

4. TITLE AND SUBTITLE
Extending Hyperspectral Capabilities with Dualband Infrared Focal Plane Arrays

5a. CONTRACT NUMBER

5b. GRANT NUMBER

5c. PROGRAM ELEMENT NUMBER

6. AUTHOR(S)
Paul D. LeVan*, John P. Hartke**, Eustace L. Dereniak***, Brian P. Beecken‡

5d. PROJECT NUMBER

5e. TASK NUMBER

5f. WORK UNIT NUMBER

7. PERFORMING ORGANIZATION NAME(S) AND ADDRESS(ES) AND ADDRESS(ES)
Photonics Research Center**
United States Military Academy
West Point, NY 10996

Physics Department‡
Bethel University
St. Paul, MN 55112

College of Optical Sciences***
University of Arizona
Tucson, AZ 85721

8. PERFORMING ORGANIZATION REPORT NUMBER

9. SPONSORING / MONITORING AGENCY NAME(S) AND ADDRESS(ES)
Air Force Research Laboratory*
Space Vehicles Directorate
3550 Aberdeen Ave SE
Kirtland AFB, NM 87117-5776

10. SPONSOR/MONITOR'S ACRONYM(S)
AFRL/VSSS

11. SPONSOR/MONITOR'S REPORT NUMBER(S)
AFRL-VS-PS-TP-2007-1008

12. DISTRIBUTION / AVAILABILITY STATEMENT
Approved for public release; distribution is unlimited. (Clearance # VS06-0851)

13. SUPPLEMENTARY NOTES
Published in the Proc of SPIE, Vol 6479, 6479OW (2007)

Government Purpose Rights

14. ABSTRACT
Dualband infrared focal plane arrays (FPA) were developed originally for multi-spectral imaging applications, where their advantages in compactness and band-to-band pixel registration, relative to conventional multi-spectral imagers, were recognized. As dualband FPA architecture is matured for quantum well and mercury cadmium telluride focal plane arrays, and becomes within the grasp of strained layer superlattice technology, applications in addition to multi-waveband imaging come to mind. In various hyperspectral applications that employ gratings, the different grating orders can sometimes be paired with the wavebands of the dual- (or multi-) waveband FPA, allowing high efficiency hyperspectral imaging over very broad wavelength regions. Exploiting the "third dimension" of FPA detecting layers for dual- and mult-waveband capability proved its usefulness for multi-waveband imaging; this paper will show similar advantages for hyperspectral applications and describe such applications.

15. SUBJECT TERMS
Focal Plane Array, Infrared, Hyperspectral

16. SECURITY CLASSIFICATION OF:			**17. LIMITATION OF ABSTRACT**	**18. NUMBER OF PAGES**	**19a. NAME OF RESPONSIBLE PERSON**: Paul LeVan
a. REPORT	**b. ABSTRACT**	**c. THIS PAGE**	Unlimited	11	**19b. TELEPHONE NUMBER** *(include area code)*
Unclassified	Unclassified	Unclassified			*505-846-9959*

Standard Form 298 (Rev. 8-98)
Prescribed by ANSI Std. 239.18

Extending hyperspectral capabilities with dualband Infrared Focal Plane Arrays

Paul D. LeVan[a], John P. Hartke[b], Eustace L. Dereniak[c], & Brian P. Beecken[d]
[a]Air Force Research Laboratory, Kirtland AFB, NM 87117-5776
[b]Photonics Research Center, United States Military Academy, West Point, NY 10996
[c]College of Optical Sciences, University of Arizona, Tucson, AZ 85721
[d]Physics Department, Bethel University, St. Paul, MN 55112

ABSTRACT

Dualband infrared focal plane arrays (FPA) were developed originally for multi-spectral imaging applications, where their advantages in compactness and band-to-band pixel registration, relative to conventional multispectral imagers, were recognized. As dualband FPA architecture is matured for quantum well and mercury cadmium telluride focal plane arrays, and becomes within the grasp of strained layer superlattice technology, applications in addition to multi-waveband imaging come to mind. In various hyperspectral applications that employ gratings, the different grating orders can sometimes be paired with the wavebands of the dual- (or multi-) waveband FPA, allowing high efficiency hyperspectral imaging over very broad wavelength regions. Exploiting the "third dimension" of FPA detecting layers for dual- and multi-waveband capability proved its usefulness for multi-waveband imaging; this paper will show similar advantages for hyperspectral applications and describe such applications.

Keywords: Hyperspectral, infrared, dualband, focal plane array

1. INTRODUCTION

There exists a long history of long slit spectrometers using conventional ("monoband") FPAs and diffraction gratings, with typically the first grating order dispersed across one dimension of the FPA, and higher orders blocked with the appropriate spectral transmission filter. These spectrometers provided good performance over an approximate octave of wavelengths, for example, within either the MWIR or LWIR. (Early slit spectrometers in the LWIR sometimes used prisms[1,2] as an alternative to gratings. The LWIR gratings at the time provided high levels of dispersion relative to then-available pixel pitches, making it difficult to disperse the entire 8 to 14 micron spectrum over full extent of the FPA, for "reasonable" spectrometer focal lengths. These prism-based systems were also optimized over a single octave of wavelength.)

Successful attempts to retain the wavelength coverage of the higher grating orders were initially achieved with cross-dispersion spectrometers for which a grating used in several orders was immediately followed by a prism, with the dispersion axes of each oriented at right angles. The prism refracts the dispersed grating spectra along the spatial axis of the FPA to separate the overlapping grating orders. Although the approach achieves a truly "broadband" (multi-octave) hyperspectral capability, some users might perceive shortcomings in the curved shape of the spectrum in a single grating order, and in the loss of spatial FOV.

The advent of dualband IR focal plane arrays (FPA) suggested a means to record two grating orders by allowing the MWIR spectrum to be recorded by the MWIR layer of the FPA, and similar for the LWIR with its grating order and FPA layer. This approach was made compelling by the realization that a grating blazed for high efficiency at

Quantum Sensing and Nanophotonic Devices IV, edited by Manijeh Razeghi, Gail J. Brown,
Proc. of SPIE Vol. 6479, 64790W, (2007) · 0277-786X/07/$18 · doi: 10.1117/12.714793

wavelength λ_o also achieves peak efficiency in the next higher grating order at a wavelength $\lambda_o/2$, and that these peak wavelengths *are dispersed by the grating at the same angle*.

The attractiveness of the approach includes the reduction in overall packaging size, when compared with a dichroic beamsplitter and a pair of gratings and FPAs for each waveband. However, it is also very advantageous for some applications to have "perfectly registered" dualband spectra that result from overlapping grating orders sampled by dualband pixels in perfect octaves of wavelength (e.g., wavelengths of λ_i & $\lambda_{i/2}$ sampled by Dualband Pixel i, with i ranging over the number of pixels).

Another promising hyperspectral approach is the Computed Tomographic Imaging Spectrometer (CTIS), which has been extensively investigated for single waveband FPAs by the University of Arizona and the Photonics Research Center at the United States Military Academy. More recently, one of us (Hartke) has pursued "dualband" CTIS concepts in the infrared, noting that the computer generated holographic (CGH) phase grating traditionally used as transmissive dispersion devices for the CTIS also has additional spectral orders that can be exploited with dualband infrared FPAs. The next section will describe a design for the dualband CTIS in a way that helps understand FPA requirements in terms of pixel format and sensitivity.

2. CTIS, OR COMPUTED TOMOGRAPHIC IMAGING SPECTROMETER

The advantage of the CTIS system is in its ability to capture all spatial and spectral axes simultaneously, i.e., in a "snapshot". Typical spectrometers such as the whiskbroom or pushbroom systems scan the scene spatially, or spectrally like in a rotating filter system. These scanning systems may not complete the scan before as a dynamic event occurs. CTIS, on the other hand, gathers all of the required information in a single integration time.

The CTIS optical system consists of four main optical elements: objective optics, collimating optics, a disperser, and a re-imaging element. The objective takes the scene and images it to the field stop. The collimator takes the light from the field stop and collimates it to pass through the disperser. After passing through the disperser the light is re-imaged to a two-dimensional detector array. (See Figure 1.)

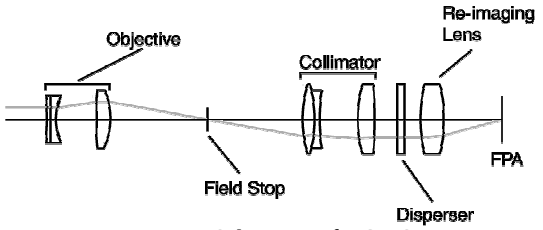

Figure 1. Schematic of a CTIS.

Key to the CTIS system is the dispersive element. The dispersive element is a computer generated holographic (CGH) etched phase grating. For visible systems the CGH is commonly made from poly-methyl methacrylate (PMMA) material etched with an electron beam. Infrared systems can use silicon, germanium, or other IR transparent medium. The dispersion of the light is achieved by changing the depth of the dispersion material and thus changing the phase of the wave front at each point. The disperser is composed of numerous unit cells. Each cell consists of an integer number (usually 8 x 8, 10 x 10 or 16 x 16) of square phasels. Each phasel is etched to a specified depth. (The term phasels is used to distinguish the cell etching of the CGH from the detector pixel on the focal plane array and the voxel, which is the three dimensional unit cell of the data cube.) The etched depth leads to a phase delay of the transmitted wavefront given by[3]

$$\Phi\lambda = \frac{2\pi d}{\lambda}(n\lambda - 1), \tag{1}$$

where Φ_λ is the phase, d is the etch depth, n_λ is the index of refraction and λ is the wavelength of the light. The λ subscript denotes the wavelength dependence of the phase and index of refraction.

The CGH modifies the incident wavefront to create the desired diffraction pattern on the focal plane. The diffraction pattern becomes the tomographic projections of the data cube. CGH are designed to create a 3 x 3, 5 x 5, or even a 7 x 7 diffraction pattern on the focal plane. When designing a CGH, we must consider the required spectral and spatial resolution, focal plane characteristics, and the object's characteristics.

The CTIS system data cube reconstruction is based on the computed tomographic techniques similar to those used in medical imaging. Computed tomography involves reconstructing a three-dimensional data cube from a series of two-dimensional projections of the object. In this system the two-dimensional projections are created by the CGH dispersive element in the collimated space of the system. The two-dimensional projections are the diffracted images of the object's image in the plane of the field stop and constitute a series of parallel projections of the three-dimensional object cube.[4] The center, or zero order projection, is a direct polychromatic image of the object. The first orders are projections through the data cube at the same angle measured from the wavelength axis. The reconstruction techniques used most often with the CTIS system are Expectation Maximization (EM)[5] and the Multiplicative Algebraic Reconstruction Technique (MART)[6]. Both techniques are iterative processes where each iteration is, in general, a better estimate of the object than the previous.

2.1 Order overlap

One of the limitations of the CTIS and other imaging spectrometers that use a diffractive element is that the range of wavelengths is limited to about a single octave. This limitation occurs because where the longer wavelengths of one diffraction order strike the focal plane at the exact same location as the shorter wavelength of the next higher order. If we consider the diffraction equation

$$m\lambda=\text{OPD}, \tag{2}$$

m is the diffraction order number and OPD is the optical path difference between two rays, we see that the diffraction maxima for m=2 and λ=1 μm occurs at the same location in the observation plane as m=1 and λ=2 μm.

A possible solution to overcoming the order overlap issue is to use prisms and filters to split the incoming light into two separate focal planes, each sensitive to a different spectral range of interest. The drawback to this approach is that the spatial co-registration of the two focal planes is difficult at best and would have to be rechecked during operation to insure there is no shift. Now if we have an interest in determining the spectral content of a scene over two separate spectral regions, we must overcome the order overlap and spatial co-registration issues. One of the most promising solutions involves use of dualband focal plane array technology.

2.2 Dualband CTIS

It is possible to overcome the order overlap limitation by using a dual band focal plane composed of detectors sensitive to a different portion of the spectrum stacked on top of each other instead of a focal plane made up of detectors with the same spectral bandpass. At the point of order overlap, each band will only respond to the incident light in their band. This also solves the spatial co-registration problem, because the two arrays of "monoband" pixels are stacked on top of each other.

As a proof-of-concept we integrated an off-the-shelf CCD camera into a CTIS system and used the blue (400 – 500 nm) and red (600 – 700 nm) spectral bands as the two bands to study.[7] The CCD camera did not have the red and blue pixels stacked on top of each other like the dualband IR detectors do. Instead the red, green, and blue sensitive pixels are in an interwoven pattern where the pixels along a row alternate red, green, and blue. In this case we can consider the red, green, and blue focal planes to be displaced from each other by one pixel. Although not perfectly co-registered, we can account for the constant difference. From our work we saw that it was possible to reconstruct to spectrally separate, spatially co-registered data cubes given the interwoven focal plane of the two detector types.

From the study we also determined how to characterize the spatial and spectral resolution of the system. The image formed on the focal plane of the CTIS system consists of a zero diffraction order in the center of the focal plane. The zero order is the direct polychromatic image of the scene imaged to the field stop. In several radial directions, determined by the CGH design, the scene's spectral content is diffracted outward as in Figure 2.

The spectral resolution of the system is determined by the extent of the zero order on the focal plane while the spatial resolution of the system is limited by the dispersion of the highest diffraction on the focal plane. Assuming the diffraction-limited spot size on the center of the focal plane is no larger than the size of the pixel, the reconstructed data cube will have the same spatial sampling as the number of pixels covered by the zero order. That is to say if the zero order covers a 100 pixel x 100 pixel area on the focal plane, the reconstructed data cube will have 100 x 100 voxels on each monochromatic plane. The resolution of the system then corresponds to the field of view subtended by each pixel. Similarly, the best spectral resolution is determined by the dispersion across the pixel in the outermost diffraction order. As an example, if the dispersion of a white light point source in the outermost diffraction order is 5 nm across the length of the pixel, the best spectral sampling we can hope for in the data cube is 5 nm.[8]

Figure 2

Figure 2. 7x7 CTIS Dispersion Pattern

Now we can apply these resolution rules-of-thumb to a dualband infrared system and demonstrate some of the practical limitations of such a system and provide some design goals for dualband IR focal planes.

Considering the spatial resolution of the system is defined by the diffraction-limited spot size and the size of the number of pixels the zero diffraction order subtends. The diffraction limited spot diameter is given by

$$D=2.44\lambda f/\#\,, \tag{3}$$

Where D is the diameter of the spot or Airy Disk, λ is the wavelength of the light and *f/#* is the system f-number. Using a pixel pitch of 25 μm as the desired diffraction limited spot diameter and 12 μm light as the longest wavelength of interest, we would need an *f/1* system or better. We can relax the diffraction limit requirement of the diffraction limited spot size only subtending a single pixel if we expand the size of the zero order on the focal plane. For example if we require 100 x 100 spatial samples of the scene then with a *f/1* system we need the zero order to subtend 100 x 100 pixels. For an *f/2* system at the same sampling we need to subtend 200 x 200 pixels. By relaxing the *f/#* of the system from *f/1* to *f/2* significantly increases the required size of the focal plane. Not only is the zero order larger, but the diffraction orders are also pushed further out on the focal plane.

For the spectral resolution of the system we will limit our system to just one diffraction order in six radial directions. We have some control over the dispersion of the CGH by changing the size of the phasels, the number of phasels in a unit cell, and the focal length of the re-imaging lens. The dispersion of the CGH is given by

$$\frac{\Delta\lambda}{\Delta x} = \frac{qx_c}{kf}, \tag{4}$$

where $\Delta\lambda/\Delta x$ is the dispersion, q is the number of phasels in a CGH unit cell, k is the diffraction order number, f is the focal length of re-imaging lens, and x_c is the length of the side of a phasel. For a particular CTIS design we predicted a dispersion of 0.5 nm/μm in MWIR and 0.75 nm/μm in LWIR.

To design an infrared system that is an f/1 system with 100 x 100 pixels in the zero order and 10 nm resolution in the MWIR and 15 nm resolution in LWIR, requires a focal plane that is at least 720 x 720 pixels if we assume a 25 μm pitch focal plane array.

The next challenge to implementing a dualband IR CTIS system is overcoming the signal to noise ratio. The signal through the CTIS system is fairly low. About 40% of the light incident on the field stop does not go into the diffraction orders because losses in diffraction efficiency. Then the light that does get into the desired diffraction orders is split into the eight first orders and the zero order. So on average less than 7% of the incident light makes it into each order. From the camera equation the irradiance on the focal plane is

$$E' = \frac{M}{4(1-m)^2 (f/\#)^2}, \tag{5}$$

where *E'* is the irradiance on the focal plane, *M* is the exitance of the spectral bandpass, and *m* is the magnification. For each diffraction order the irradiance is then on average 7% of the value calculated in equation (5). This relatively low signal must be considered in the development of dualband focal plane arrays for use by the CTIS system, since it emphasizes higher sensitivity at lower levels of FPA irradiance (E').

3. GENERAL COMMENTS ON DUALBAND INFRARED FOCAL PLANE ARRAYS

Dualband FPAs have been realized in various "waveband pairs", including MWIR-MWIR, MWIR-LWIR, and LWIR-LWIR. Unlike conventional single waveband FPAs, each pixel is a site for dualband detection. The shorter waveband material absorbs shorter wavelength photons, and transmits longer wavelength photons to the (deeper) longer waveband layer. Typically, the photocurrent for each waveband is injected separately into the detector multiplexer circuit, and integrated at a separate charge storage site within the multiplexer. Dualband FPAs have been fabricated for both "simultaneous" operation, for which both photocurrents are integrated during the same frame time and typically over at least part of the same integration time, and "sequential" operation, for which one waveband is integrated during one frame time, the other waveband during the next frame time. In the case of sequential operation, the frames of data from the FPA are typically "waveband interlaced". Waveband-specific values of integration time are easy to implement in the sequential configuration, but exact simultaneity is no longer possible.

Dualband FPA formats in the range of 320x256 dualband pixels are common. Larger dualband formats in HgCdTe are reportedly underway (Dr Paul Norton, private communication), enabling the 720x720 CTIS goals described above. More recently, a 1024x1024, dualband quantum well infrared photodetector (QWIP) effort has been initiated[9]. Additional details dualband IRFPAs can be found in Reference 10 and perhaps in more recent publications.

In general, the broad wavelength coverage of dualband FPAs comprising photovoltaic detectors is amenable to dispersive spectral imaging. In the case of photovoltaic dualband devices of HgCdTe, vapor phase epitaxial growth of the detector material allows for tailoring of the depth profile of both "x" in $Hg_{1-x}Cd_xTe$ and doping density, and therefore of the cutoff wavelengths of the two diodes. The LWIR layer is grown on top of the MWIR layer. The substrate for the dualband film growth is transparent in both the MWIR & LWIR, thereby allowing the resulting IRFPA to be "back-illuminated", with MWIR photons absorbed first, and LWIR photons passing through the MWIR layer (as

through a long-pass spectral filter) and being absorbed near the deeper LWIR junction. Alternate fabrication approaches begin with separate "growths" of the shorter and longer waveband detector material, followed by the interconnection of these with the detector multiplexer using etched vias. Although this approach results in a "front illuminated" dualband FPA, the shorter waveband is still "seen" first by incoming photons, as for the vapor phase approach. This front illuminated FPA type is the basis for the spectrometer described below[11].

4. LONG SLIT SPECTROMETER USING A DUALBAND FPA

Traditional gratings have the well-known property of providing multiple, overlapping orders. As mentioned above, the existence of overlapping orders has been viewed as a liability for most applications, for which unwanted orders falling within the range of useable detector response would corrupt the single grating order of interest.

The attractive feature about the higher grating orders that is relevant to multi-octave spectral imaging concepts relates to their having similar peak wavelength efficiencies as the first order. Specifically, a (perfect) grating with first-order blaze wavelength λ_B has peak efficiencies near λ_B / n in grating order n. These higher order wavelengths are diffracted by the grating at the same angle, and the higher order spectra lay on top of the first order spectrum. Combining the advantage of overlapping grating orders with the capability of multi-waveband FPAs to integrate spectra independently in the various orders allows us to achieve efficient multi-octave spectral imaging in a compact way.

Data obtained with a laboratory demonstration of the "dualband spectrometer" concept is described in Reference 11; its analysis presented no insurmountable obstacles, and anomalies in applying a blackbody-derived calibration found for discrete wavelength regions were shown to result from spectral contamination issues. These anomalies are mitigated with the selection of proper FPA cut-off wavelengths and by employing a long-pass filter that blocks grating orders higher than second. These suggestions have been implemented in the latest configuration, which we now describe.

The spectrometer (upgraded with an FPA having cut-off wavelengths near 5 and 10.5 microns, with the spectrometer providing spectral coverage from approximately 3.7 to 6.2 and 7.3 to 12.3 microns) was used in August 2006 to collect spectral images of the Sun. Collection of such images is made compelling by comparing the solar angular diameter (~0.5 degree) with the length of the spectrometer slit (~1 degree), from which it can be seen that both edges of the solar disk can be simultaneously viewed over the full range of spectrometer wavelengths.

Having determined the prospects for solar observations in the infrared, it became important to find a way to filter the harmful levels of visual and near infrared radiation while preserving the optical quality of the infrared observations. The selection of a full-aperture solar filter was motivated by amateur astronomical observations of the sun at visual wavelengths (where the solar flux needs to be attenuated by many orders of magnitude to prevent eye damage). The filtering approach needs to preserve the high angular resolution of relatively large-aperture, diffraction-limited (or seeing-limited) observations. However, the level of infrared transmission is largely unknown for the available solar filters (including optical quality Black Polymer from Thousand Oaks Optical in CA, and black Mylar from several sources). We therefore acquired Black Polymer and performed a wavelength scan in the infrared using a commercial FTS system. A quantity of material sufficient to cover the ~17 cm fore-optics diameter was implemented on the basis of the FTS scan shown in Figure 3 below.

Figure 3 revealed narrow waveband regions in both the MWIR and LWIR where useful spectral data could be collected. Combined with known atmospheric absorption features (including CO_2 from ~4.1 to ~4.5 um; O_3 from ~9.3 to ~9.8 um), the Black Polymer transmission results in strong infrared solar signal appearing in wavelength regions evident in the spectral image of the Sun shown in Figure 4; the corresponding wavebands are described in Table 1.

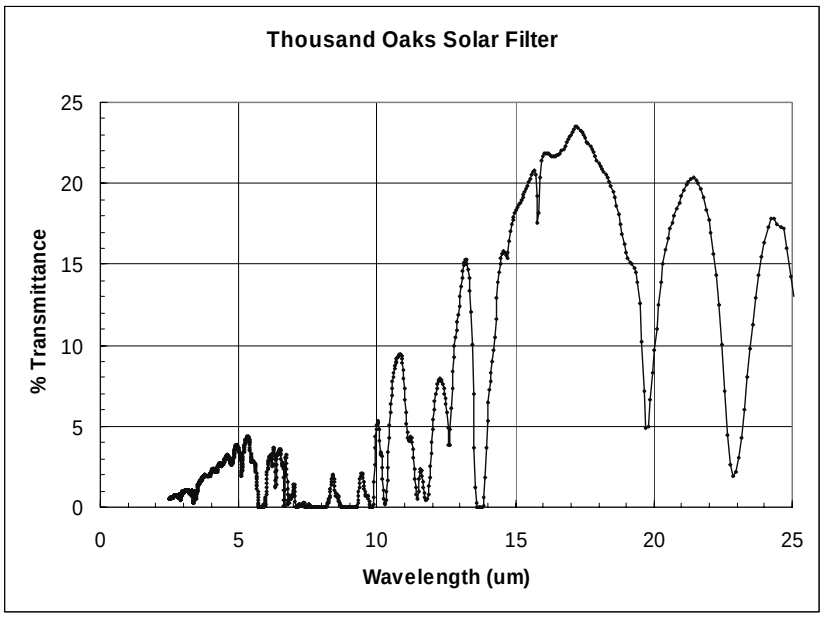

Figure 3. Transmission spectrum of Black Polymer collected at AFRL**.**

Our solar observations took place during the afternoon of 11 August 2006. The observing mode placed the spectrometer on a manual tripod. The sun was visually sighted through solar filter material and then acquired in the infrared with minor tripod adjustments along the narrow extent of the spectrometer slit. We then offset the slit to the "leading edge" of the Sun corresponding to a geometrical chord of shortened length within the slit. Allowing the

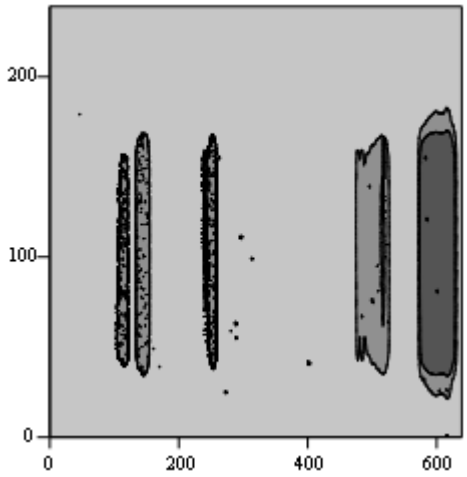

imagedisp^{T}

Figure 4. Dualband spectral image of a chord of the solar disk. Shorter wavelengths are towards the right, with the horizontal axis ticks of 0, 200, 400, and 600 corresponding to wavelengths of 12.3, 9.14, 5.51, and 3.94 um, respectively, with a break in the scale at 320. The scale of the vertical axis is approximately 72 microrad (15 arcsec) per pixel. Although the image shows a side-by-side display of the MWIR & LWIR spectra, the FPA employed has a 320x240, dualband pixel format; the spectral images are "stacked" at the time of acquisition.

Table 1. System wavebands for Spectrometer Observations with Black Polymer (BP)

Waveband designation	Approximate center wavelength (um)	Approximate Half widths (um)	Comments
MW_short	~3.9	3.8 to 4.1	Atmos. CO_2 limits on long wavelength side
MW_long	~4.6	4.5 to 4.7	Atmos. CO_2 limits on short wavelength side
LW_short	~8.3	8.2 to 8.5	(BP transmission peak near 9.6 um offset by atmos. O_3 absorption)
LW_long	~10	9.9 to 10.1	BP transmission peak near 10.5 limited by declining HCT response

Earth's rotation to generate motion of the slit across the solar disk resulted in a growth in the solar extent to the diametric value that was followed by a decline; we continuously collected spectral images over the Sun's transit of the slit. This approach allowed observations of maximum angular extent corresponding to a solar diameter in a way that "point and shoot" observations would not, due to the difficulty of precisely orienting the slit along the solar diameter in an instant of time.

The visual diameter of the sun on the date of observation (at distance of 1.014 astronomical units) is 1894 seconds of arc, according to the Solar Ephemeredes. This value corresponds to between 125 and 126 pixel IFOVs, using the design value of 15 arcsec for the IFOV (as verified with observations of a distant blackbody of known aperture diameter). Shown in Figure 5 is a MWIR spatial scan near the solar diameter, for which the FWHM was found to be in the range of 108 to 110 pixels; the source of the discrepancy between the observed infrared and tabulated visual widths is under investigation.

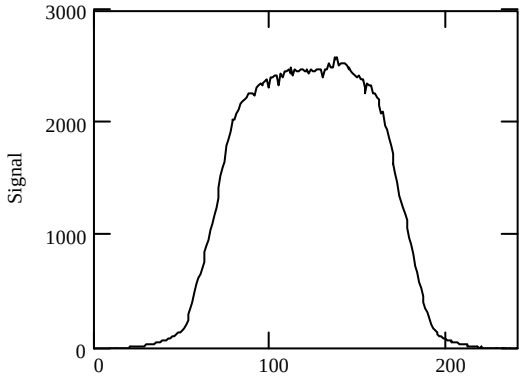

Figure 5. MWIR spatial profile of Sun, observed on 11 August. The pixel IFOV is approximately 15 arcsec, and the wavelength of the scan is approximately 3.9 um.

These solar observations do not explore the full potential of the grating-based dualband spectrometer – they are spectrally uncalibrated, in the sense that the overall spectrometer response, including that of the black polymer, has not been calibrated with a blackbody source. They are also limited in spectral coverage to the relatively narrow "transmission" features of the Black Polymer. We hope to remedy the former issue by conducting a spectral calibration

of the type described in Reference 11, with a hot blackbody used to overcome the attenuation in the black polymer. This spectral calibration would also allow the accurate profiling of atmospheric absorption features falling within the useable wavelengths of the Black Polymer. Nevertheless, we still find the observations presented here useful in many ways. They strongly confirm the utility of the spectrometer for sources extended on the scale of fractions of a degree.

5. OTHER PROSPECTIVE HYPERSPECTRAL APPROACHES ENABLED BY DUALBAND FPAS

Note also that at least one other spectral approach lends itself well to dual- and eventual multi-waveband FPA applications – specifically, the Fabry-Perot (FP) interferometer. The spacing of the etalons in the FP determines the peak wavelength that is transmitted, making the device useful for high spectral resolution, wavelength-scanning spectrometers. The FP also transmits integer subdivisions of wavelength that are typically blocked for traditional applications; alternatively, these could be retained, detected, and kept separated by a dual- or multi-waveband FPA. The very high spectral resolution of the FP would stress IR FPA performance because of the small values of photocurrent produced, but these FP applications may be enabled as dualband FPAs approach higher sensitivity (and uniformity) at lower flux levels.

We note in passing that broad spectral coverage is possible with an alternative approach using conventional, "monoband" FPAs and gratings "tailored" with concentric zones of differing facet pitch, thereby extending the range in wavelength for which first-order blaze efficiency is appreciable. These gratings are typically electron beam etched. The approach is noteworthy in its application of existing FPA technology; its shortcoming may be the difficulty with a spectrometer design that spreads multiple octaves of wavelength over many pixels, for which the minimization of spectral "smile" and keystone, important for many applications, is made more difficult.

In the more distant future, multiwaveband FPAs are expected to provide an increase in multi-spectral information at the pixel level without the need for dispersive elements. Presently, demonstrations with three wavebands exist (based on the separate growths of detector layers mentioned previously). As the number of wavebands increases to the point of providing spectral overlap of adjacent spectral resolution elements, hyperspectral capability is achieved by the FPA by itself. This technology may someday become possible through grading of composition in photovoltaic or superlattice detectors so that photons of different wavelength are continuously absorbed at different depths, and their resulting photocurrents are isolated with a vertical grid of contacts or perhaps even vertically-implanted junctions.

ACKNOWLEDGEMENTS

We acknowledge Dr John Hubbs and Diana Maestas-Jepson of Ball Aerospace for helpful conversations and acquisition of the laboratory spectral scans of the black polymer material.

REFERENCES

1. J. A. Hackwell, D.W. Warren, et al., "A low resolution array spectrograph for the 2.9 to 13.5 micron spectral region", *Proc. of SPIE* Vol. 1235, 171-180 (1990).
2. P. D. LeVan, "Capabilities of the AFGL Mosaic Array Spectrometer", *Publication of Astronomical Society of the Pacific*, Vol. 102, 190-199 (1990).
3. C.E. Volin, "Portable snapshot infrared imaging spectrometer", Ph.D. Dissertation, University of Arizona, pp. 32-37 (2000).
4. G. T. Herman, *Image Reconstruction from Projections, The Fundamentals of Computerized Tomography*, Academic Press, New York (1980).
5. L. A. Shepp, Y. Vardi, "Maximum likelihood reconstruction for emission tomography." in *IEEE transactions on medical imaging*, Vol. MI-1, No. 2, pp. 113-122 (Oct 1982).
6. A. Lent, "A convergence algorithm for maximum entropy image restoration." in *Image analysis and evaluation, SPSE conference proceedings*, Rodney Shaw, ed., pp. 249-257 (Jul 1976).

7. J. Hartke, E.L. Dereniak, "Hyperspectral-dual spectral region imaging spectrometer", *Proc. of SPIE* Vol. 5563, pp. 156-166 (2004).
8. J. Hartke, E.L. Dereniak, and P.D. LeVan, "Non-scanning dual infrared band hyperspectral imaging spectrometer design", *Proc. of SPIE* 6295, 62950D (2006).
9. S. D. Gunapala, et al., "Towards Dualband Megapixel QWIP Focal Plane Arrays", *Proceedings of International Workshop on Quantum Well Infrared Photodetectors, QWIP 2006*, Kandy, Sri Lanka (Jun 2006)
10. P. D. LeVan , "Perspectives on Dualband Infrared Focal Plane Array efforts", *Proc. of SPIE* Vol. 5563, 130 (2004).
11. P.D. LeVan & D. Maestas, "A 3.5 to 12 Micron "Dualband" Spectrometer", *Optical Engineering* Vol 43, No. 12, page 3045 (2004).